

VOLCANIC ASH CLOUD OBSERVATION USING
GROUND-BASED KA-BAND RADAR AND NEAR-
INFRARED LIDAR CEILOMETER DURING THE
EYJAFJALLAJÖKULL ERUPTION*Marzano, F. S., et al.*

Volcanic ash plumes are formed during explosive volcanic eruptions. After advection over several thousands of kilometers, volcanic ash particles are highly fragmented, dispersed and aged with micron-sized sorting. This Annex describes the ash microphysical modeling and the simulated radar and lidar signatures.

A.1. VOLCANIC ASH MICROPHYSICAL MODELING

In this work all particles are assumed to be spheroids, i.e. ellipsoids with circular symmetry. This shape is, on the one hand, quite general and, on the other hand, simplifies the numerical treatment of scattering. Similarly to what described in Marzano et al. (2012), we set up a microphysical model of ash particle distributions. This means to specify: a) particle size distribution (PSD); b) particle ellipsoidal axial ratio (AR); c) particle orientation distribution (POD); d) particle density and dielectric constant. Ash PSDs are typically modeled through a normalized Gamma or Weibull size distribution [e.g., Marzano et al., 2006; 2010]. In case of a multi-mode size distribution, it is always possible to suppose more than one analytical PSD, characterized by different mean sizes and total number of particles. In this study, we have adopted the scaled Gamma (SG) PSD as a general model for all particles. If D_e is the diameter of a spherical volume-equivalent particle, the scaled-Gamma PSD N_p [$\text{mm}^{-1}\text{m}^{-3}$] for a generic class of ash particles p can be written as:

$$N_p(D_e) = N_{np} \left(\frac{D_e}{D_{np}} \right)^{\mu_p} e^{-\Lambda_{np} \left(\frac{D_e}{D_{np}} \right)} \quad (1)$$

where the “intercept” parameter N_{np} and the “slope” parameter Λ_{np} in a logarithmic plane are related to the “shape” parameter μ_p and to the particle density ρ_p through:

$$N_{np} = 10^6 \frac{6C_p \Lambda_{np}^{\mu_p+4}}{\pi \rho_p D_{np}^4 \Gamma(\mu_p+4)}; \quad \Lambda_{np} = \mu_p + 1 \quad (2)$$

with C_p the mass concentration [g/m^3] and D_{np} [mm] the number-weighted mean diameter. PSD in (1) is completely specified by the three parameters μ_p , D_{np} and C_p (with a particle density ρ_p between 1 and 2.5 g/cm^3). If particles are sphere equivalent, their mass is $m_p = \rho_p (\pi/6) D_e^3$.

The *number of ash classes* with respect to their average size is set to 5 as follows: i) very fine ash (VA) with mean equivalent diameters uniformly distributed between 2³-2³ μm (0.125-8 μm); ii) fine ash (FA) between 2³-2⁶ μm (8-64 μm); iii) coarse ash (CA) between 2⁶-2⁹ μm (64-512 μm); iv) small lapilli (SL) between 2⁹-2¹² μm (0.512-4.096 mm); and finally v) large lapilli (LL) between 2¹²-2¹⁵ μm (4.096-32.768 mm). With respect to previous studies [Marzano et al., 2012], we have added the class of large lapilli and very fine ash to take into account ballistic fallout as well as dispersed small particles in order to deal with a fairly general observation scenario (closer to and farther from the volcanic vent). Moreover, uniform distribution around the mean size has been assumed instead of Gaussian probability.

Each diameter class may be subdivided with respect to other main parameters, e.g. the ash concentration and orientation angle [Marzano et al., 2012]. The following sub-sets have been introduced:

- i) 4 classes of ash concentration, i.e.: very small (VC), small (SC), moderate (MC), and intense (IC) concentrations. These sub-sets are eventually compacted into 1 class uniformly going from 10⁻⁶ g/m^3 up to 10 g/m^3 ;

- ii) 5 classes of particle orientation with Gaussian POD characterized by a mean canting angle θ_m , i.e.: tumbling with $\theta_m=30^\circ$ (TO.1), tumbling with $\theta_m=45^\circ$ (TO.2), tumbling with $\theta_m=60^\circ$ (TO.3), oblate $\theta_m=0^\circ$ (OO); prolate $\theta_m=90^\circ$ (PO). These 5 sub-sets are reducible to 3;
- iii) 2 classes of AR models, i.e.: ratio basaltic-andesitic (RB) and ratio rhyolitic (RR), even though we have here selected only the RB case;
- iv) 3 classes of VA, FA, CA spherical particles (SP) with all 5 concentrations.

Particle dielectric constant models have been derived from literature; in particular, their dependence on SiO_2 weight W_{SiO_2} and relative humidity fraction (RH) is derived from the available data [e.g., Adams et al., 1996; Shettle and Fenn, 1971]. Ash classes can exhibit a mixed-phased permittivity due to liquid and ice water in the atmosphere. Particle classes with a mixed refractive index have been also introduced [Marzano et al., 2010]. In such a case, we have limited our attention to particles smaller than lapilli, so that 3 new mixed-phase classes have been labeled by VAm, FAm, CAm for all 5 concentrations. Liquid and ice water particle classes (e.g., cloud droplets, ice crystals, snowflakes) can be added to generalize the scenario. Considering all combinations, the nominal number of classes is 233 ($5 \cdot 4 \cdot 5 \cdot 2 + 15 + 15 + 3$) which can be effectively reduced to 20 ($5 \cdot 1 \cdot 3 \cdot 1 + 3 + 2$), as we will discuss later on in this work.

A.2. VOLCANIC ASH PARTICLE SCATTERING AND EXTINCTION

The conditions allowing for the Rayleigh scattering regime, depending on particle refraction index and the ratio between the particle diameter and the incident wavelength λ , are not always satisfied by the characteristics of the problem under discussion. Simulated polarimetric radar observables for spheroidal particles can be obtained by using the T-matrix numerical method [Mishchenko et al., 1996], implemented through the

Hydrometeor Ash Particle Ensemble Scattering Simulator (HAPRESS) [Marzano et al., 2012].

In order to simulate the optical polarimetric signatures of volcanic particles we have included within HAPRESS the geometrical optical limits which cannot be evaluated by T-matrix code due to numerical convergence problems [Min et al, 2003; Gasteiger et al., 2011]. In the next sub-sections we will introduce observables related to backscattering amplitude since those related to forward scattering phase are beyond the scopes of this paper [see Marzano et al., 2012].

Polarimetric radar observables

Using horizontal (h) and vertical (v) polarization states, copolar (Z_{hh}, Z_{vv}) and crosspolar (Z_{vh}, Z_{vh}) radar reflectivity factors can be expressed in terms of ash PSD. If λ is the wavelength associated to a given frequency f , K_p is the ash particle radar dielectric factor and θ is the particle canting angle, $S_{xy}^{(b)}$ are the backscattering components at x ($x=h,v$ for the receiving mode) and y ($y=h,v$ for the transmitting mode) polarization of the complex scattering matrix S , we can define:

$$Z_{xy}(f) = \frac{\lambda^4}{\pi^5 |K_p|^2} \int_0^\pi \int_0^\infty 8\pi^2 |S_{xy}^{(b)}(D_e, \phi, f)|^2 N_p(D_e) p_p(\theta) dD_e \sin \theta d\theta = \frac{\lambda^4}{\pi^5 |K_p|^2} \langle 4\pi S_{xy}^{(b)}(D_e, \theta) \rangle \quad (3)$$

In (3) angle brackets stands for average over PSD N_p and POD p_p , assuming a uniform azimuthally symmetric POD [Marzano et al, 2012]. Note that: i) $Z_{hv}=Z_{vh}$ for cross-polarization reciprocity; ii) the canting angle θ is defined in the polarization plane with respect to its vertical polarization unit-vector; iii) if Z_{xy} is expressed in $[\text{mm}^6\text{m}^{-3}]$, then $Z_{XY}=10\log_{10}(Z_{xy})$ is conventionally expressed in dBZ.

The derived differential reflectivity Z_{dr} , which is the ratio of reflectivity at the two polarization states, and the linear depolarization ratio L_{dr} are defined as:

$$Z_{dr}(f) = \frac{Z_{hh}(f)}{Z_{vv}(f)}; \quad L_{dr}(f) = \frac{Z_{hv}(f)}{Z_{hh}(f)} \quad (4)$$

where Z_{dr} and L_{dr} are unitless and usually expressed in dB. The specific power attenuation α_{hh} (α_{vv}) at polarization h (v) can be obtained from:

$$\alpha_{xy}(f) = 2\lambda \text{Im} \left[\langle 4\pi S_{xy}^{(f)}(D_e, \phi, f) \rangle \right] \quad (5)$$

The apex “ f ” of S indicates its forward components. Note that, if α_{xy} is in $[\text{km}^{-1}]$, the above quantities are usually defined in dB within the radar community $\alpha_{XY} = 4.343 \alpha_{xy}$.

Note that, if the ellipsoidal axial ratio shows an intrinsic variability, the particle non-sphericity can significantly affect the differential reflectivity Z_{dr} . The L_{dr} is not dependent on the particle concentration and it is governed by the inverse of reflectivity-weighted axial ratio within the Rayleigh scattering. The L_{dr} signature will then increase with increasing canting angle and axial ratio variability.

Polarimetric lidar observables

The lidar backscattering coefficients β_{hh} , β_{vv} and β_{vh} at horizontal (h) and vertical (v) polarization states can be expressed similarly to the corresponding radar coefficients. Indeed, from (4) their definition can be written as:

$$\beta_{xy}(\lambda) = \int_0^\pi \int_0^\infty 4\pi \left| S_{xy}^{(b)}(D_e, \phi, \lambda) \right|^2 N_p(D_e) p_p(\phi) dD_e \sin \phi d\phi = \langle 4\pi S_{xy}^{(b)}(D_e, \phi) \rangle \quad (6)$$

where $x=h,v$ again stands for the receiving mode and $y=h,v$ for the transmitting mode polarization. Note that β_{xy} is usually expressed in $[\text{km}^{-1}\text{sr}^{-1}]$ so that $\beta_{XY} = 10 \log_{10}(\beta_{xy})$ is here conventionally expressed in dB β (in analogy to dBZ for Z_{XY}).

The same applies to the specific attenuation or extinction coefficient α_{xy} , which similarly to (5) is expressed in $[\text{km}^{-1}]$ and is defined as:

$$\alpha_{xy}(\lambda) = 2\lambda \text{Im} \left[\langle 4\pi S_{xy}^{(f)}(D_e, \phi, \lambda) \rangle \right] \quad (7)$$

Analogously to (7), if α_{xy} is in $[\text{km}^{-1}]$, $\alpha_{XY} = 4.343 \alpha_{xy}$ is conventionally expressed in dB. Similarly to Z_{dr} and L_{dr} in (4), the unitless lidar linear co-polarization ratio δ_v and cross-polarization ratio δ_r can be defined by:

$$\delta_v(\lambda) = \frac{\beta_{vv}(\lambda) - \beta_{hh}(\lambda)}{\beta_{vv}(\lambda) + \beta_{hh}(\lambda)}; \quad \delta_r(\lambda) = \frac{\beta_{vh}(\lambda)}{\beta_{hh}(\lambda)} \quad (8)$$

Radar and lidar polarimetric signatures

In order to discuss combined polarimetric signatures, we have considered existing radar and lidar instrument setups, e.g. zenith-pointing Ka-band radars and colocated lidars operating at 355 nm, 532 nm and 1024 nm wavelength [e.g., Madonna et al., 2010]. HAPSS outputs have been validated for volcanic ash with numerical simulations available in literature [e.g. Wiegner et al., 2009].

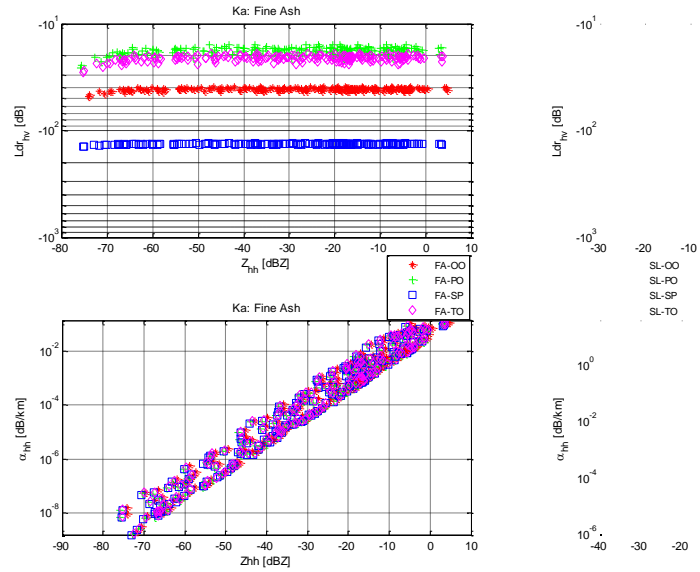


Figure 1a: Correlation between zenith Ka-band polarimetric radar observables in terms of copolar reflectivity $Z_{hh}(36\text{GHz})$, linear depolarization ratio $L_{dr}(36\text{GHz})$, and specific attenuation $\alpha_{hh}(36\text{GHz})$ for FA size class, using all ash concentrations classes (VC, SC, MC and IC) and for different particle orientations (OO, PO, SP and TO.2) with basaltic axial ratio model.

This section illustrates examples of ash sub-classes, limited here for brevity to FA signatures in terms of Ka-band and near infrared (NIR) polarimetric observables (which are used for the combined system introduced later on). Figure 1a shows how $Z_{hh}(36\text{GHz})$ correlates to linear depolarization $L_{dr}(36\text{GHz})$ and specific power attenuation $a_{hh}(36\text{GHz})$. Note that the particle orientation has an impact on $L_{dr}(36\text{GHz})$, with the OO (mainly horizontal with respect to the ground) providing values of about -40 dB. Specific attenuation is pretty low for FA (lower than 0.15 dB/km), but larger of 1 dB/km for larger particles. In figure 1a we have also added the behavior of spherical particles (SP) where we expect theoretically $Z_{hv}=0$ and $L_{dr}=0$.

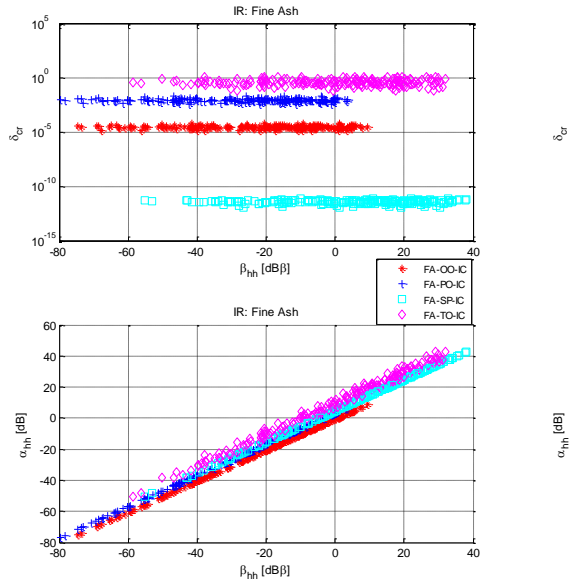


Figure 1b: Same as in the Figure 1a panels, but for the zenith lidar copolar backscatter coefficient $\beta_{hh}(1064\text{nm})$, linear cross-polarization ratio $\delta_{cr}(1064\text{nm})$, and extinction coefficient $\alpha_{hh}(1064\text{nm})$ with relative humidity ranging between 30 and 70%.

In Figure 1b panels show the correlation between zenith-pointing NIR backscatter coefficient $\beta_{hh}(\lambda)$, linear cross-polarization ratio $\delta_{cr}(\lambda)$, and extinction coefficient $\alpha_{hh}(\lambda)$ for fine ash. Note that $\beta_{hh}(1064\text{nm})$

ranges from -80 to -10 dB β for FA-PO and -40 to 40 dB β for FA-SP, whereas the sensitivity to orientation is no more evident for the larger particles. The extinction $\alpha_{hh}(1064\text{nm})$ ranges from -80 to 40 dB/km for FA, whereas $\alpha_{hh}(1064\text{nm})$ from -110 to -10dB/km for larger particles. It is worth noting that if $\beta_{hh}(\lambda)$ increases with increasing ash concentration C_p , it decreases with increasing particle mean diameter D_n , a behavior which is explained by the optical limit regime of scattering taking place at NIR for particles larger than few microns [Wiegner et al., 2009; Min et al., 2003]. On the opposite, the radar reflectivity $Z_{hh}(f)$ increases with the increase of both C_p and D_n .

REFERENCES

- [Adam et al. 1996] Adams, R., et al. (1996). Measurements of the complex dielectric constant of volcanic ash from 4 to 19 GHz. J. Geophys. Res., vol. 101, pp. 8175–8185.
- [Ferguson and Stephens 1983] Ferguson, J. A., and Stephens, D. H. (1983). Algorithm for inverting lidar returns. Appl. Opt., 22, 3673-3675.
- [Gudmundsson et al. 2012] Gudmundsson, M. T., et al. (2012). Ash generation and distribution from the April-May 2010 eruption of Eyjafjallajökull, Iceland, NG Scientific report, 2 : 572 | DOI: 10.1038/srep00572.
- [Marzano et al. 2012] Marzano, F. S., et al. (2012). Synthetic Signatures of Volcanic Ash Cloud Particles from X-band Dual-Polarization radar, IEEE Trans. Geosci. Rem. Sens., 50, 193-211.
- [Marzano et al. 2013] Marzano, F. S., et al. (2013). Inside Volcanic clouds: Remote Sensing of Ash Plumes Using Microwave Weather Radars. Bulletin Am. Met. Soc., 1567-1586, DOI: 10.1175/BAMS-D-11-00160.1.
- [Min et al. 2003] Min, M., et al. (2003). Scattering and absorption cross sections for randomly oriented spheroids of arbitrary size, J. Quant. Spectr. Rad. Transfer, 79–80, 939–951.

[Mishchenko et al., 2002] Mishchenko, M. I., et al. (2002). *Scattering, absorption and emission of light by small particles*, Cambridge University Press, Cambridge (USA).

[O'Dowd et al. 2012] O'Dowd, C., et al. (2012). The Eyjafjallajökull ash plume- Part I: Physical, chemical and optical characteristics., *Atmos. Env.*, 48, 129-142.

[Shettle and Fenn 1979] Shettle, E. P., and Fenn R. W. (1979). *Models for the Aerosol of the Lower Atmosphere and the Effect of Humidity Variation on their Optical Properties*. AFGL-TR-79-0214 Environmental research papers no.076.

[Wiegner et al. 2009] Wiegner, M., et al. (2009). Numerical simulations of optical properties of Saharan dust aerosols with emphasis on lidar applications, *Tellus*, 61B, 180-194.